JOURNAL OF COMPUTATIONAL PHYSICS 57, 391–402 (1985)

Application of Orthogonal Mapping to Some Two-Dimensional Domains

E. D. CHIKHLIWALA AND Y. C. YORTSOS

Departments of Chemical and Petroleum Engineering, University of Southern California, Los Angeles, California 90089-1211

Received September 22, 1983; revised January 3, 1984

1. INTRODUCTION

Recent advances in the numerical generation of orthogonal, body-fitted, curvilinear coordinates [1] have provided powerful methods which can be potentially applicable to the study of the deformation of an interface in moving boundary problems. Of particular promise appears to be a method recently proposed by Ryskin and Leal [2] for the numerical generation of orthogonal mappings. We elected to investigate the applicability of this technique to 2D geometrical domains likely to arise in immiscible fluid–fluid displacement processes in porous media.

Such processes are macroscopically characterized by the existence of two single-phase regions, containing displacing and displaced phases, respectively, separated by an advancing two-phase zone of variable fluid content, the width of which decreases with an increase in the displacement velocity. At high displacement rates, the transition zone can be adequately approximated on a macroscopic level by an abrupt interface [3], on each side of which single-phase Darcy flow occurs (Fig. 1).

Following the approach in [2] we consider mapping the physical regions on each side of the interface, at a fixed time, into rectangular regions by an orthogonal

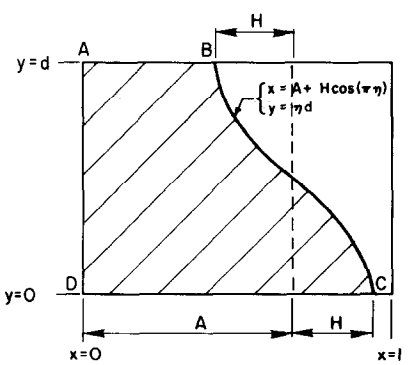

FIG. 1. Physical regions in immiscible displacement processes.

0021-9991/85 $3.00

transformation determined numerically by the method of weak constraint [2]. This paper presents the numerical results obtained in our attempt to generate an orthogonal mapping for typical geometries of the region occupied by the displacing phase (ABCDA in Fig. 1), the mapping for the other region being obtained by an identical procedure.

2. Numerical Procedure

According to [2] a two-dimensional orthogonal mapping $(x, y) \to (\xi, \eta)$ can be obtained from the solution of the grid generating equations

$$\frac{\partial}{\partial \xi}\left[f \frac{\partial x}{\partial \xi}\right]+\frac{\partial}{\partial \eta}\left[\frac{1}{f} \frac{\partial x}{\partial \eta}\right]=0 \tag{1a}$$

$$\frac{\partial}{\partial \xi}\left[f \frac{\partial y}{\partial \xi}\right]+\frac{\partial}{\partial \eta}\left[\frac{1}{f} \frac{\partial y}{\partial \eta}\right]=0 \tag{1b}$$

$$0<\xi, \eta<1,$$

where the shape factor f is defined by

$$f(\xi, \eta)=\frac{h_\xi}{h_\eta} \tag{2a}$$

$$h_\xi^2=\left(\frac{\partial x}{\partial \xi}\right)^2+\left(\frac{\partial y}{\partial \xi}\right)^2 \tag{2b}$$

$$h_\eta^2=\left(\frac{\partial x}{\partial \eta}\right)^2+\left(\frac{\partial y}{\partial \eta}\right)^2. \tag{2c}$$

The above system of equations was discretized using finite differences in a staggered grid. The resulting vector equation

$$\mathbf{A} \cdot \mathbf{u}=\mathbf{b}, \tag{3}$$

where $\mathbf{A}$ is a symmetric, pentadiagonal, coefficient matrix, $\mathbf{u}$ the coordinate vector $\begin{bmatrix} x \\ y \end{bmatrix}$ and $\mathbf{b}$ the vector specified by the boundary conditions, was subsequently solved by the iterative process [4]

$$u_{i+1,j}^n=u_{i,j}^n-\frac{\omega}{a_3}\left[a_1 u_i^{n+1}{}_{,j}+a_2 u_{i,j+1}^n+a_3 u_{i,j}^n\right.$$

$$\left.+a_4 u_i^{n+1}{}_{,j-1}+a_5 u_{i-1}{}^{n+1}{}_{,j}\right]. \tag{4}$$

Here a_1, a_2, a_3, a_4, a_5 are coefficients involving f, while ω is the relaxation parameter. Details on the numerical algorithm employed can be found in [5]. After

each cycle, consisting of updating the values of x and y by applying one or more SOR passes, the values of f at the boundaries are determined. We use Eq. (2) on boundaries where Dirichlet conditions are specified (fixed positions of the boundary points), or an a priori distribution on boundaries where Neumann conditions are specified (zero normal derivatives), as an extra degree of freedom is available in the latter case. Values of f in the interior are then obtained using the algebraic interpolation suggested in [2]

$$\begin{aligned} f(\xi, \eta) = {} & (1-\xi) f(0, \eta) + \xi f(1, \eta) + (1-\eta) f(\xi, 0) + \eta f(\xi, 1) \\ & - (1-\xi)(1-\eta) f(0, 0) - (1-\xi)\eta f(0, 1) \\ & - \xi(1-\eta) f(1, 0) - \xi\eta f(1, 1). \end{aligned} \tag{5}$$

For the generation of orthogonal grids of satisfactory accuracy, various cases involving different boundary condition specifications were studied. In all cases, Dirichlet boundary conditions for the coordinates x and y were specified on the boundaries *BC*, *DA*, and *AB*, *BC*, *CD*, respectively. When a complete boundary correspondence was prescribed (Case A) Dirichlet conditions were specified on all boundaries. We also investigated the cases when boundary correspondence was prescribed on *BC*, *CD*, *DA* (Case B), or when boundary correspondence was prescribed on boundary *BC* only (Case C). In the latter cases, Neumann conditions on x and y were used, where appropriate, to ensure orthogonality. Table I summarizes the boundary conditions imposed in each investigation.

The equation of the interface was typically represented in the parametric form

$$\begin{aligned} \mathbf{x} &= A + H \cos \pi\eta \\ \mathbf{y} &= d\eta. \end{aligned} \tag{6}$$

Parameters A, H control the location and inclination of the interface, respectively (hence the severity of the expected effect of density differences in the displacement

TABLE I

Boundary Conditions

Boundary	Case A	Case B	Case C
AB	x—Dirichlet y—Dirichlet	x—Neumann y—Dirichlet	x—Neumann y—Dirichlet
BC	x—Dirichlet y—Dirichlet	x—Dirichlet y—Dirichlet	x—Dirichlet y—Dirichlet
CD	x—Dirichlet y—Dirichlet	x—Dirichlet y—Dirichlet	x—Neumann y—Dirichlet
DA	x—Dirichlet y—Dirichlet	x—Dirichlet y—Dirichlet	x—Dirichlet y—Neumann

process), while d denotes the aspect ratio of the geometry studied. Since the inclination of the interface is expected to increase as time progresses, the above representation allows for a stringent test of the ability of the proposed technique to generate satisfactory orthogonal grids for shapes likely to arise in the displacement process. Base case studies were carried out by fixing the parameter values to $A = 0.75$, $d = 1$. The orthogonality of the grid was tested by evaluating at all nodal points the angle θ between two intersecting grid lines according to the expression

$$\cos\theta = \frac{x_\xi x_\eta + y_\xi y_\eta}{(x_\xi^2 + y_\xi^2)^{1/2}(x_\eta^2 + y_\eta^2)^{1/2}}. \tag{7}$$

At the point in the (ξ, η) space where maximum deviation from orthogonality occurs, the index $\text{MDO} = |\pi/2 - \theta|$ was selected to represent the orthogonality characteristics of the numerical grid. Convergence was reached when the index MDO at a fixed point stabilized within one decimal point to a constant value.

3. Results and Discussion

This section contains the numerical results obtained for different boundary condition specifications. In each investigation, the relaxation parameter ω and the shape factor specification on boundaries where Neumann conditions are prescribed were suitably optimized as described in detail below.

Case A. When complete boundary correspondence was prescribed, Dirichlet conditions on the variables x and y were specified along the boundaries of the region. Various choices of boundary correspondence were studied ranging from equally spaced to exponential nodal distributions. To attain coordinate spacing control the interpolation formula for the shape factor (5) was multiplied by the control function $(1\text{-}k \sin\pi\xi \sin\pi\eta)$. Within the range of our investigation (k varying from 0.2 to 0.9) no satisfactory orthogonal grid was obtained. In particular, in most of the simulations attempted, the numerical solution did not converge, while in cases where convergence was obtained, the orthogonality condition was not satisfactory (e.g., $\text{MDO} = 40°$, for $H = 0.15$ in a 16×16 grid, exponential nodal distribution on AB, CD, equidistant on BC, AD).

These results should be compared to those previously reported for the case of complete boundary correspondence. In Figs. 7 and 8 of [2] an orthogonal grid in the interior of a region containing an axis on symmetry is obtained, using an equally spaced boundary nodal distribution. Our experience indicates that the success of the weak constraint method in producing orthogonal grids in this case is primarily attributed to the symmetry of the region. We were able to produce very satisfactory results by simulating the symmetric region consisting of the base case and its mirror image across the axis AB with equidistant nodal distribution along the boundaries (Fig. 2). A low value of the maximum deviation from orthogonality resulted, $\text{MDO} = 3.7°$, for $H = 0.15$ in a 16×16 grid.

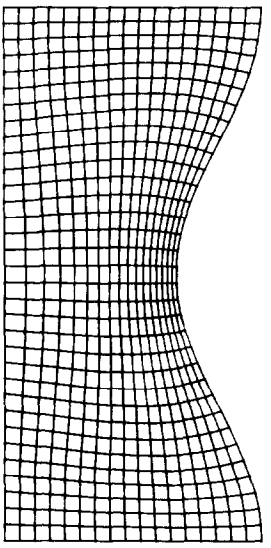

FIG. 2. Orthogonal grid for symmetric region, Case A, $H = 0.15$, 16×32 grid.

We conjecture that orthogonal grids of good accuracy given a complete boundary correspondence can be obtained by the weak constraint method, provided that the region under consideration contains a symmetry element and the specified boundary nodal distribution is accordingly symmetric. On the other hand, generation of accurate orthogonal grids for non-symmetric regions (such as *ABCDA* in Fig. 1) requires that the boundary nodal distribution in some boundaries is left unspecified, as outlined in the following cases.

Case B. In this investigation Neumann conditions were specified on the x coordinate at the boundary AB, while Dirichlet conditions following equidistant nodal distribution were specified on all other boundaries.

$$\begin{aligned} \mathbf{x} &= A\xi && \text{on } CD \\ \mathbf{y} &= d\eta && \text{on } BC,\ DA \\ \mathbf{x} &= A + H\cos\pi\eta && \text{on } BC. \end{aligned}$$

Along the course of this investigation it was observed that Case B produced results consistently better than those in the previous case. Convergence was always obtained, while for a particular specification of the shape factor on the boundary AB, the maximum deviation from orthogonality varied from 1.3° to 6.5° as H varied from 0.05 to 0.25 in a 16×16 grid. A typical orthogonal grid generated is shown in Fig. 3.

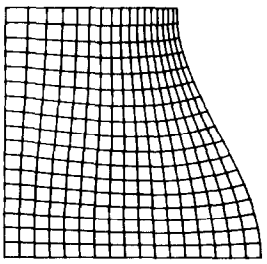

FIG. 3. Orthogonal grid, Case B, $H = 0.15$, 16×16 grid.

Three different representations for f on the boundary AB were studied:

(i) constant shape factor distribution

$$f(\xi, 1) = 1,$$

(ii) linear shape factor distribution

$$f(\xi, 1) = f(0, 1) + [f(1, 1) - f(0, 1)]\xi$$

and

(iii) exponential shape factor distribution

$$f(\xi, 1) = f(0, 1) + [f(1, 1) - f(0, 1)] \frac{\exp[K\xi] - 1}{\exp[K] - 1},$$

where K is an arbitrary parameter.

Maximum deviation from orthogonality values for various choices of the shape factor distribution are summarized in Table II. It is noticed that both linear and exponential distributions result in considerably more accurate orthogonal grids as compared to a constant distribution. The case of linear variation of f on AB produces orthogonal grids of good accuracy for all values of H studied. On the other hand, exponential distribution simulations, although more accurate at low values of H, fail to generate orthogonal grids for $H = 0.25$.

TABLE II

Effect of Shape Factor Distribution (Case B)[a]

$f(\xi, \eta)$	$H = 0.05$	$H = 0.10$	$H = 0.15$	$H = 0.20$	$H = 0.25$
Constant	10.1°	52.0°	—	—	—
Linear	1.3°	2.4°	3.7°	5.0°	6.5°
Exponential ($K = 0.8$)	1.3°	2.2°	3.2°	7.1°	—

[a] $A = 0.75$, $d = 1.0$, $\omega = 1.8$, 16×16 grid.

TABLE III

Effect of Shape Factor Distribution (Case C)[a]

$f(\xi, \eta)$	$H = 0.05$	0.10	0.15	0.20	0.25
AB linear *CD* linear *DA* linear	0.3°	1.0°	2.0°	3.6°	5.7°
AB exponential *CD* linear *DA* exponential	0.4°	0.9°	2.1°	4.0°	6.8°
AB exponential *CD* exponential *DA* exponential	0.4°	0.9°	1.9°	3.6°	5.8°

[a] $A = 0.75$, $d = 1.0$, $\omega = 1.8$, 16×16 grid.

Case C. In the absence of boundary correspondence, Neumann conditions for the x and y coordinates were specified on the boundaries *AB*, *CD*, and *DA*, respectively, while a boundary nodal distribution was prescribed on boundary *BC* only ($y = d\eta$, $x = A + H \cos \pi\eta$). Orthogonal grids of excellent accuracy were obtained for typical values of the system parameters. A significant improvement in accuracy over both Cases A and B was observed for all values of H (Table III). As in Case B, best results were obtained by specifying a linear or exponential shape factor distribution on the boundaries *AB*, *CD*, *DA*. Typical orthogonal grids generated in this case are shown in Figs 4, 5, and 6.

Using Case C with a linear shape factor distribution as a base case, sensitivity studies on the effect of various parameters were further carried out. The effect of grid size on the orthogonality achieved, the total number of iterations, and the computational time required on a computer DEC KL10 are shown in Table IV. It is noticed that the maximum deviation from orthogonality decreases with an increase in size, although the improvement in accuracy becomes marginal beyond a certain value. Thus, although the SOR iterative scheme is $O(h^2)$, the error introduced by the weak constraint method appears not to be a sensitive function of

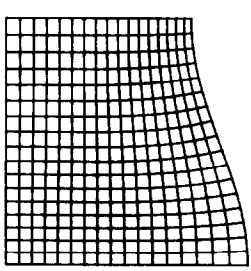

FIG. 4. Orthogonal grid, Case C, $H = 0.10$, 16×16 grid.

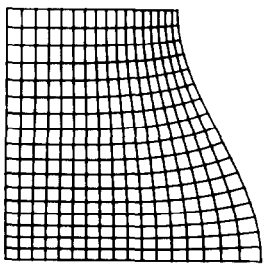

FIG. 5. Orthogonal grid, Case C, $H = 0.15$, 16×16 grid.

h within the range of our investigation. On the other hand, the number of iterations and CPU time required for convergence increase significantly with the number of grid nodes n, the latter varying in a fashion roughly proportional to $n^{2.8}$, as anticipated [5].

Table V summarizes the effect of the aspect ratio on the maximum deviation from orthogonality. As expected, maximum deviations for fixed values of H are larger in narrow, long regions (small aspect ratio). The accuracy in orthogonality increases monotonically with the aspect ratio, although beyond a certain value of d in the range 0.75–1.00, further increase in the aspect ratio has a marginal effect on the grid orthogonality. On the other hand, for the low value $d = 0.25$, the rate of convergence is slow, while the orthogonality achieved, at the maximum allowable number of iterations, is rather poor.

For completeness, a study to determine the optimum relaxation factor in the iterative scheme employed was also carried out. Due to the large size of the coefficient matrix an explicit evaluation of the maximum eigenvalue is not feasible, thus a numerical investigation was undertaken. Results obtained are plotted in Fig. 7. In accordance with theoretical predictions, there exists an optimum value of the relaxation factor (~ 1.8), corresponding to a three-fold decrease in the number of iterations required for convergence as compared to very low (1.1) or very high (1.94) values. The curve in Fig. 7 is representative of typical SOR schemes where the number of iterations rises sharply as the value of ω deviates from its optimum

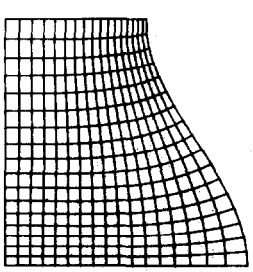

FIG. 6. Orthogonal grid, Case C, $H = 0.20$, 16×16 grid.

TABLE IV

Effect of Grid Size (Case C)[a]

Grid size	MDO	Number of iterations	CPU time (sec)
8^2	1.6°	18	1.68
16^2	2.0°	14	4.68
24^2	1.7°	20	13.72
32^2	1.4°	33	38.39
40^2	1.1°	42	75.54
48^2	1.0°	66	173.57

[a] $A = 0.75$, $d = 1.0$, $H = 0.15$, $\omega = 1.8$.

TABLE V

Effect of Aspect Ratio (Case C)[a]

Aspect ratio	MDO	Number of iterations
0.25	21.7°	126
0.50	4.9°	19
0.75	2.3°	16
1.00	2.0°	14
1.25	1.8°	13
1.50	1.6°	13
2.00	1.3°	13
3.00	1.1°	17
5.00	0.8°	13

[a] $A = 0.75$, $H = 0.15$, $\omega = 1.8$, 16×16 grid.

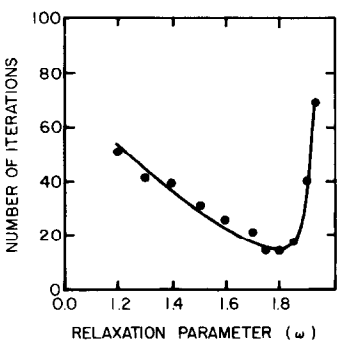

FIG. 7. Effect of relaxation parameter on the number of iterations, Case C, 16×16 grid.

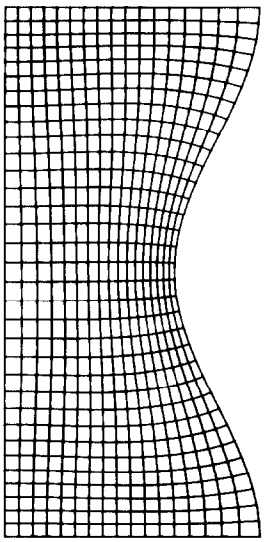

FIG. 8. Orthogonal grid, Case C, $H = 0.15$, $d = 2.0$, 16×32 grid.

value. No significant effect of the value of the relaxation factor on orthogonality was noticed.

To conclude this investigation, a parallel study was carried out to test the applicability of the weak constraint method in symmetric regions using the boundary nodal specification of Case C. Numerical simulations were carried out for the region obtained by reflection of the domain *ABCDA* (Fig. 1) about the *AB* axis. A sharp increase in accuracy (MDO = 0.6°) was obtained for the base case ($A = 0.75$, $d = 2.0$, $H = 0.15$, 8×16 grid, $\omega = 1.8$, linear shape factor distribution), as compared to the accuracy obtained using the boundary correspondence of Case A (MDO = 5.2°). A typical grid for this case is shown in Fig. 8. Although the number of iterations increased by almost a factor of two, the resulting substantial increase in accuracy suggests that specification of Neumann boundary conditions whenever possible is preferred over complete boundary correspondence for the generation of

TABLE VI

Effect of Curvature in Symmetric Regions (Case C)[a]

H	MDO	Number of iterations	CPU time (sec)
0.05	0.5°	12	3.42
0.10	0.8°	18	4.42
0.15	0.6°	35	7.66
0.20	1.4°	32	7.11

[a] $A = 0.75$, $d = 2.0$, $\omega = 1.8$, 8×16 grid.

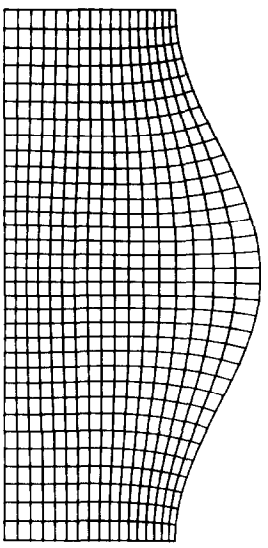

FIG. 9. Orthogonal grid, Case C, $H = -0.15$, $d = 2.0$, 16×32 grid.

good orthogonality grids. At this point, it should also be mentioned that the grids obtained for such symmetric regions have orthogonality characteristic slightly better (Table VI) than the grids generated for the non-symmetric region *ABCDA* with identical boundary correspondence and grid size (e.g., MDO $= 0.6°$ for symmetric regions, 16×16 grid, compared to MDO $= 1.6°$ for non-symmetric region, 8×16 grid).

Finally, the region shown in Fig. 9, obtained by reflection of the domain of Fig. 1 about the axis *CD*, was also simulated. It was found that good orthogonal grids were generated. However, the accuracy in a 16×16 grid was considerably lower (MDO $= 2.7°$) compared to the grid of Fig. 8.

4. CONCLUSIONS

In this article we presented numerical results obtained from the application of the method of weak constraint [2] for the generation of orthogonal coordinates in physical regions likely to arise in immiscible displacement processes in porous media.

The numerical scheme of successive overrelaxation employed did not produce orthogonal grids of good accuracy for typical non-symmetric regions given arbitrary complete boundary correspondence, although good orthogonality resulted in symmetric regions with a symmetric boundary correspondence. By contrast, orthogonal grids of excellent accuracy are obtained for non-symmetrical regions by

specifying a complete boundary nodal distribution (Dirichlet conditions) on one of the boundaries, while leaving the boundary correspondence unspecified (Neumann conditions) on the other boundaries.

The accuracy in orthogonality in a strong function of the domain geometry and the specification of shape factor distribution on the boundaries. A linear shape factor distribution and symmetric regions were generally found to result in grids of higher accuracy. Sensitivity studies indicate that grid size spacing, although strongly influencing the rate of convergence, appears to have a marginal effect on orthogonality control.

It is anticipated that orthogonal mapping using the method of weak constraint can be successfully applied in the numerical simulation of typical immiscible displacement processes in porous media.

ACKNOWLEDGMENTS

The authors would like to acknowledge the valuable contribution from Professor W. Proskurowski, Department of Mathematics, University of Southern California, and useful suggestions by the reviewers on the marginal manuscript.

REFERENCES

1. J. F. THOMPSON, F. C. THAMES, AND C. W. MASTIN, *J. Comput. Phys.* **15** (1974), 299.
2. G. RYSKIN AND L. G. LEAL, *J. Comput. Phys.* **50** (1983), 71.
3. J. BEAR, "Dynamics of Fluids in Porous Media," Chap. 9, Elsevier, New York, 1972.
4. L. A. HAGEMANN AND D. M. YOUNG, "Applied Iterative Methods," Academic Press, New York, 1982.
5. E. D. CHIKHLIWALA, "Immiscible Liquid—Liquid Displacement in Porous Media," M.Sc. thesis, University of Southern California, 1983.